This is a preprint of the paper published in JVSTB. Citation: Afanas'ev et al. // Journal of Vacuum Science & Technology B **33**, 03D101 (2015). DOI: 10.1116/1.4907228

Photo-electron Spectra of finite thickness layers

Viktor P. Afanas'ev,[1] Olga Y. Golovina,[1] Alexander S. Gryazev,[1] Dmitry S. Efremenko,[2] and Pavel S. Kaplya[1]
[1)] *National Research University "Moscow Power Engineering Institute", Department of General Physics and Nuclear Fusion, Moscow, 111250, Krasnokazarmennaya 14, Russia*
[2)] *Deutsches Zentrum fuer Luft- und Raumfahrt (DLR), Institut fuer Methodik der Fernerkundung (IMF), 82234 Oberpfaffenhofen, Germany*

A method of computing X-ray photo-emission spectra in the wide range of energy losses and different sighting angles is presented. Photo-emission spectra for layers of finite thickness are investigated. Angular and energy spectra are analyzed using the invariant imbedding principle. They are computed using the small-angle approximation and the exact numerical solution of the multiple photo-electron scattering problem in solids. The presented methods of X-ray photo emission spectra analysis are compared regarding their efficiencies. The comparison of the exact numerical solution to those based on the straight line approximation and the small angle approximation reveals an error of the straight line approximation of about 50%. Numerical solutions are compared with the experimental data and Monte-Carlo simulations.

I. INTRODUCTION

X-ray photo-electron spectroscopy (XPS) is one of the most effective tools for surface analysis[1,2]. XPS analysis is based on the estimation of the area under the peak, which is due to elastically scattered electrons with a specific characteristic energy. The area under the peak is related to the amount of a certain element in the near-surface layer. The thickness of this layer is approximately equal to the inelastic mean free path (IMFP). This method is called "peak shape analysis", which uses an appropriate software for XPS spectra processing to identify the quantitative composition of the sample[3]. A common approach for data processing is based on the straight line approximation (SLA) in which multiple elastic scattering processes[4,5] are neglected. In contrast to the SLA, the small-angle approximation (SAA) takes into account multiple elastic scattering events which change significantly the electron movement direction and that small angle scattering events are more probable than those corresponding to larger angles.

More accurate sample depth profiling method using PES spectra measured in the energy loss range of about 100 eV or more can be designed. Tougaard[2,6,7] showed that different surface morphology compositions of the multilayer system produce the same elastic peak intensities but with different energy losses in the rest of the spectral range. In these cases a common methodology for peak shape analysis based on the SLA can lead to significant errors. However, this phenomenon demonstrated in[2,6,7] is qualitatively correct and has to be considered.

The SLA approach[1–5] is widely used mainly due to its simplicity. In general, the SLA should be considered as a technique providing qualitative but not quantitative results, because the inelastic cross section and the elastic cross section are of the same order. Usually the influence of elastic scattering on the XPS signal is taken into account by using the transport approximation[1,2,8] or the Monte-Carlo (MC) method[1,2]. As stated in[9], the transport approximation leads to a significant error while MC simulations are time-consuming. Under such circumstances it is not efficient to solve the inverse problem using the fitting procedure based on these techniques. The same problems arise in satellite remote sensing of the atmosphere for the retrieval of atmospheric constituents from reflected spectra. A method for solving the radiative transfer problem relies on the discrete ordinate formalism[10,11]. On the other hand, approximate methods based on analytical approaches are less time-consuming. The small-angle approximation belongs to this category and was proposed by Goudsmit and Saunderson[12,13] for computing transmission functions for electrons scattered in solids. In this paper, we apply this technique to the photo-electron transport problem, and show that it leads to smaller errors than the SLA. The transport approximation is used in the radiative electron transfer problem when the particle's path length exceeds the transport range l_{tr}[14]. The results obtained using the SLA and the SAA will be compared with the exact numerical solution of the boundary value problem for the transport equation.

We consider the multiple inelastic scattering process based on the Landau's theory[15]. In order to describe PES it is necessary to consider the sample as a multilayer system described by different energy loss laws in surface and bulk layers. The retrieval of inelastic differential cross sections in the bulk $\omega_{inB}(\Delta)$ and surface layers $\omega_{inS}(\Delta)$ is the most important part of the XPS energy loss spectrum reconstruction. The most effective method of the differential inverse inelastic mean free path (DIIMFP) and differential surface excitation parameter (DSEP) retrieval which is an an ill-posed problem by

nature[19] is based on the reflection electron energy loss spectroscopy (REELS) [16–18].

In[20,21] so-called intrinsic plasmon excitations are introduced. They are considered as additional non-local processes of inelastic photo-electron energy losses and are related only to the photo-ionization process. In this paper only DIIMFP and DSEP (shown in Fig. 2) retrieved from the REELS experimental data are used for PES calculations. The intrinsic excitation processes are not included in the model.

The boundary value problem for the photo-electron transport equation is solved by using the invariant imbedding technique[9,14,24]. The description of sequential XPS spectra, as given in[9], requires the solution of a set of equations for the reflection $R(z,\Delta,\Omega_0,\Omega)$, transmission $T(z,\Delta,\Omega_0,\Omega)$ and photo-electron emission flux density $Q(z,\Delta,\Omega_0,\Omega)$ functions, where z is the layer thickness, $\Delta = E_0 - E$ is the electron energy loss, $\Omega_0 = (\mu_0,\varphi_0)$, $\Omega = (\mu,\varphi)$ are the incident and sighting angles, respectively. The solution of these equations will be found numerically by using the small-angle approximation[9,24].

II. BASIC THEORY: EQUATIONS FOR Q_k AND R_k FUNCTIONS

Let us introduce the functions Q_k/R_k which are the photo-electron flux density function and the reflection function of particles that have experienced exactly k inelastic scattering events, respectively. Then, in a wide range of energy losses, the functions Q and R are expanded into series of Q_k and R_k functions, respectively, as follows:

$$\begin{aligned} &Q(z,\Delta,\Omega_0,\Omega) = Q_0(z,\Omega_0,\Omega)\,\delta(\Delta) \\ &+\sum_{k=1}^{\infty}\left[Q_k(z,\Omega_0,\Omega)\,x_{in}^k(\Delta)\right] \end{aligned} \tag{1}$$

and

$$\begin{aligned} &R(z,\Delta,\Omega_0,\Omega) = R_0(z,\Omega_0,\Omega)\,\delta(\Delta) \\ &+\sum_{k=1}^{\infty}\left[R_k(z,\Omega_0,\Omega)\,x_{in}^k(\Delta)\right], \end{aligned} \tag{2}$$

with

$$\begin{aligned} &x_{in}^1(\Delta) = x_{in}(\Delta), \\ &x_{in}^{k+1}(\Delta) = \int_0^{\Delta} x_{in}^k(\Delta-\varepsilon)\,x_{in}(\varepsilon)\,d\varepsilon. \end{aligned} \tag{3}$$

Here, the Q_k and R_k functions refer to the k-fold inelastically scattered particles. If the differential single scattering inelastic cross section $x_{in}(\Delta)$ (DIIMFP or DSEP) stands for the energy spectrum which is observed after the single inelastic scattering event, then the k-fold convolution $x_{in}^k(\Delta)$ identifies the energy losses spectrum after k successive inelastic scattering events.

The main advantage of the invariant imbedding method consists in the fact that we can obtain equations for the expansion coefficients Q_k, R_k and T_k avoiding the computations of the path length distribution function (PLDF).

Below the following notations are used: n is the atomic density, $\omega_{el}(\mu',\mu,\varphi')$ and σ_{el} are the differential cross section and the total cross section of elastic scattering, respectively, $\omega_{in}(E_0,\Delta)$ and σ_{in} are the differential cross section and the total cross section of inelastic scattering, respectively, $\sigma_{x\to e}$ is the total cross section of photo-ionization, $x_{in}(E_0,\Delta) = \omega_{in}(E_0,\Delta)/\sigma_{in}$ is the normalized differential inverse inelastic mean free path (NDIIMFP), $x_{el}(\mu',\mu,\varphi') = \omega_{el}(\mu',\mu,\varphi')/\sigma_{el}$ is the normalized differential elastic cross section, $\mu = \cos(\theta)$, θ is the polar angle and φ is the azimuthal angle.

The normalization conditions for x_{in} and x_{el} are given by

$$\begin{aligned} &\int_0^{E_0} x_{in}(E_0,\Delta)\,d\Delta = 1, \\ &\int_0^{2\pi}\int_{-1}^{1} x_{el}(\mu_0,\mu',\varphi')\,d\mu'd\varphi' = 1, \end{aligned} \tag{4}$$

respectively. Also, we introduce the single scattering albedo and the photo-ionization albedo, respectively as follows:

$$\lambda = \frac{\sigma_{el}}{\sigma_{in}+\sigma_{el}};\ \lambda_\gamma = \frac{\sigma_{x\to e}}{\sigma_{in}+\sigma_{el}}.$$

The angular distribution of photo-electrons $f(\mu_0,\mu,\varphi)$ produced by an excited atom is expanded in a series of Legendre polynomials

$$f(\mu_0,\mu,\varphi) = \frac{1}{4\pi}\sum_{i=0}^{3}\beta_i P_i(\theta), \tag{5}$$

where P_i is the Legendre polynomial. Then, the photo-electron-emitting source[27,28] is

$$F(\mu_0,\mu,\varphi) = \sigma_{x\to e} f(\mu_0,\mu,\varphi) \tag{6}$$

Here $\sigma_{x\to e}$ is the photo-ionization cross section.

The equations for the emitted photo-electron flux density have been derived in[9]. To obtain the equation for $Q_k(z,\mu_0,\mu,\varphi)$, we add a layer of thickness dz above the layer of thickness z and consider the corresponding changes of Q_k. The thickness dz is chosen small enough to neglect multiple scattering in this layer. The final differential equation is given by

$$\begin{aligned} &\tfrac{\partial}{\partial\tau}Q_k(\tau,\mu_0,\mu,\varphi) + \tfrac{1}{\mu}Q_k(\tau,\mu_0,\mu,\varphi) \\ &-\tfrac{(1-\lambda)}{\mu}Q_{k-1}(\tau,\mu_0,\mu,\varphi) = \delta_{k0}\lambda_\gamma f(\mu_0,\mu,\varphi) \\ &+\lambda_\gamma f\otimes R_k + \lambda Q_k\otimes x_{el}\lambda Q_k\otimes x_{el}\otimes R_0 \\ &+\lambda\sum_{m=0}^{k-1} Q_{k-m}\otimes x_{el}\otimes R_m, \end{aligned} \tag{7}$$

where $\tau = (\sigma_{el}+\sigma_{in})\,nz$, and

$$Q_k \otimes x_{el} = \int_0^{2\pi}\int_0^1 Q_k\left(\tau,\mu_0,\mu',\varphi'-\varphi\right)\cdot x_{el}\left(\mu',\mu,\varphi'\right)\frac{d\mu'}{\mu'}d\varphi' \quad (8)$$

A detailed derivation of (7) can be found in[9].

The electron density function Q_0 identifies photoelectrons which escape into the vacuum without being scattered inelastically. They produce the elastic peak with the corresponding characteristic energy. Applying the SLA to Eq. (7) leads to

$$\begin{aligned}&\frac{\partial}{\partial\tau}Q_k\left(\tau,\mu_0,\mu,\varphi\right)+\frac{1-\lambda}{\mu}Q_k\left(\tau,\mu_0,\mu,\varphi\right)=\\&=\delta_{k0}\lambda_\gamma f\left(\mu_0,\mu,\varphi\right)+\\&\quad+\left(1-\delta_{k0}\right)\frac{(1-\lambda)}{\mu}Q_{k-1}\left(\tau,\mu_0,\mu,\varphi\right).\end{aligned} \quad (9)$$

The solution of equation (7) in the small-angle approximation is obtained by using the spherical harmonic method[24]. As the differential elastic scattering cross-section is strongly forward peaked, the integral terms in (7) can be simplified as follows:

$$\begin{aligned}&\frac{\partial}{\partial\tau}Q_k^{m,l}+\frac{\left(1-\lambda x_{el}^l\right)}{\mu}Q_k^{m,l}=\\&\quad=\lambda_\gamma\delta_{k0}F^l+\left(1-\delta_{k0}\right)\frac{(1-\lambda)}{\mu}Q_{k-1}^{m,l}.\end{aligned} \quad (10)$$

Equation (7) and the simplified equations (9-10) are first order linear differential equations. The solution of (7) in conjunction with (10) can be expressed as

$$\begin{aligned}Q_k=\sum_{l=0}^{\infty}\sum_{m=0}^{l}&\frac{2l+1}{2}P_l\left(\mu_0\right)P_l\left(\mu\right)\cdot\\&\cdot Q_k^{m,l}\cos\left[m\left(\varphi-\varphi_0\right)\right],\end{aligned} \quad (11)$$

where

$$\begin{aligned}Q_k^{m,l}=\mu\frac{\lambda_\gamma F^{m,l}}{1-\lambda x_{el}^{m,l}}\left[\frac{1-\lambda}{1-\lambda x_{el}^{m,l}}\right]^k\cdot\\\cdot\left[1-\exp\left(-\frac{1-\lambda x_{el}^{m,l}}{\mu}\tau\right)\cdot\sum_{n=0}^{k}\left(\frac{1-\lambda x_{el}^{m,l}}{\mu}\tau\right)^n\frac{1}{n!}\right].\end{aligned} \quad (12)$$

Here, x_{el}^l are the expansion coefficients of the normalized elastic cross section in terms of Legendre polynomials, while F^l are the expansion coefficients of the differential cross section of photoelectric ionization in terms of Legendre polynomials.

In the SAA (11), the changes of the electron movement direction from downward to upward and vice versa are neglected due to the fact that $x_{el}\left(\pi\right)/x_{el}\left(0\right)\ll 1$. To obtain the exact solution, we have to take into account the reflection processes (the 2nd and the 4th terms in Eq. (7)) and to use the equation for the reflection function $R\left(\tau,\Delta,\mu_0,\mu,\varphi\right)$[24]. The functions $R_k\left(\tau,\mu_0,\mu,\varphi\right)$ for the flux of reflected electrons after k inelastic scattering events are given by

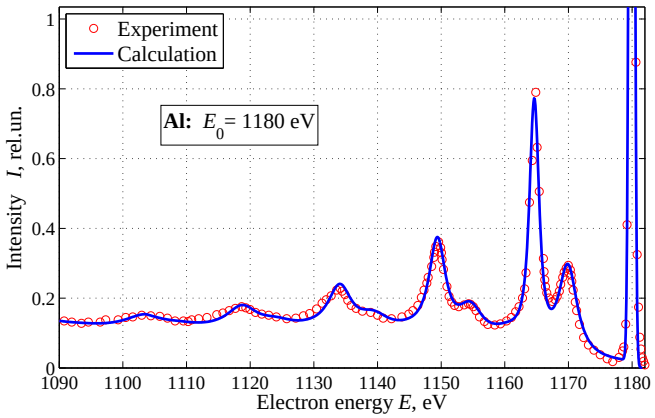

FIG. 1. (Color online) REELS spectra for Al with the initial electron energy $E_0 = 1180$ eV. Measurements are taken from [16] while calculations are performed using Eqs. (2) and (13).

$$\begin{aligned}&\frac{\partial}{\partial\tau}R_k\left(\tau,\mu_0,\mu,\varphi\right)+\left(\frac{1}{\mu_0}+\frac{1}{\mu}\right)R_k\left(\tau,\mu_0,\mu,\varphi\right)\\&=\lambda x_{el}+\lambda x_{el}\otimes R_k+\lambda R_k\otimes x_{el}\\&+\lambda R_0\otimes x_{el}\otimes R_k+\lambda R_k\otimes x_{el}\otimes R_0\\&+\lambda\sum_{j=1}^{k-1}R_{k-j}\otimes x_{el}\otimes R_j\\&+\left(1-\lambda\right)\left(\frac{1}{\mu_0}+\frac{1}{\mu}\right)R_{k-1}\left(\tau,\mu_0,\mu,\varphi\right).\end{aligned} \quad (13)$$

Eqs. (7) and (13) can be solved numerically using the Backward Differential Formula – BDF[29]. The BDF method converts equation (7) into the algebraic Riccati equation if $k=0$, or into the Lyapunov equation if $k>0$. Equation (13) is reduced to a system of linear equations.

The inaccuracy of Q_k determined by Eqs. (7) and (13) is caused by uncertainties in the differential elastic scattering cross section $\omega_{el}\left(\mu_0,\mu,\varphi\right)$ and the single scattering albedo λ. Nowadays a lot of reliable information on the elastic cross sections $\omega_{el}\left(\mu_0,\mu,\varphi\right)$[30] is available. Much effort has been put into the improvement of the database for total cross sections of inelastic scattering[31,32]. However, the retrieval of the DIIMFP and the DSEP is still a challenging task [16,17,25,26]. In modern methods of cross section reconstruction[16,17], the inelastic cross sections are represented as a superposition of surface excitations and bulk excitations with appropriate weights. This is shown in Fig. 2.

For fitting we use the experimental REELS dataset which is shown in Fig. 1. The retrieved DIIMFP for Al is shown in Fig. 2. Calculations were performed using Eq. (2) with coefficients R_k being the solution of Eq. (13). The DIIMFP data are used for PES spectrum calculations as shown in Fig. 3. The coefficients Q_k for the surface and bulk layers are calculated via the numerical solution of Eq. (7). Calculations of PES and REELS spectra are performed with the 2-layer model which has been described in detail in[33]. No intrinsic excitation processes are taken into account for XPS spectra calculations.

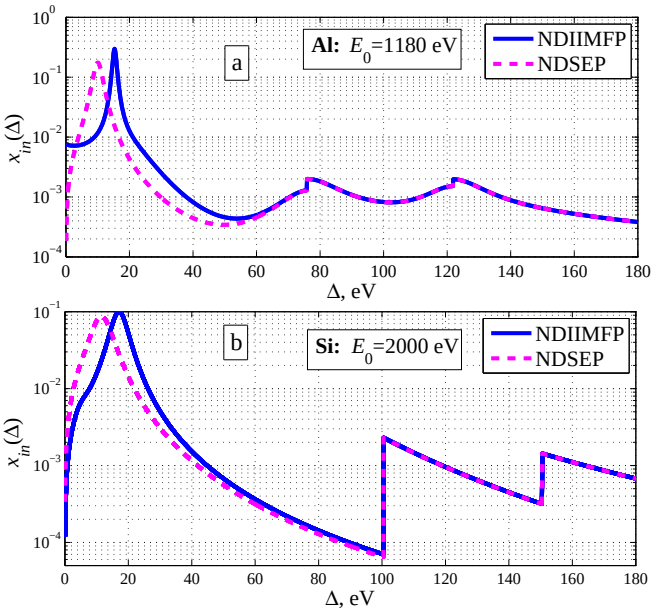

FIG. 2. (Color online) Retrieved NDIIMFP and NDSEP for (a) Al and (b) Si.

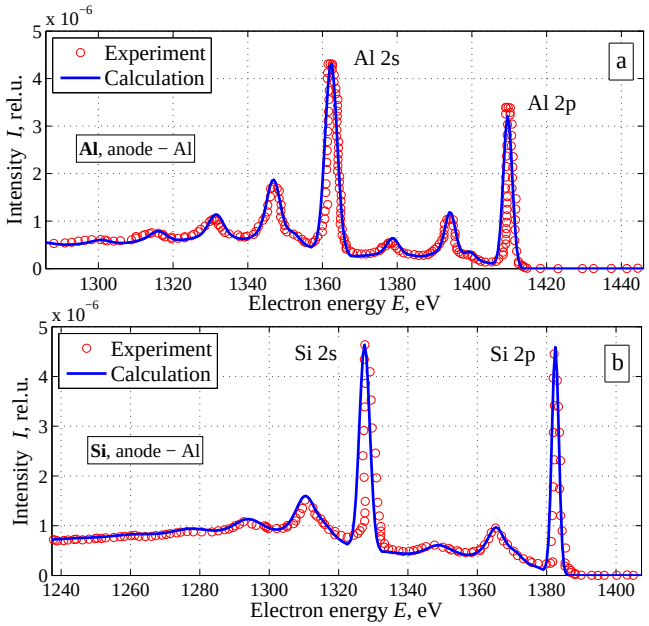

FIG. 3. (Color online) PES spectra of (a) Al and (b) Si excited with Al$K\alpha$ radiation. The measurements are taken from[34], while the Q-functions (1) are computed using Q_k, which is the exact numerical solution of Eq. (7).

The differential inelastic scattering cross sections $x_{in}(\Delta)$ are approximated by

TABLE I. Fitting parameters for NDIIMFP and NDSEP.

	Al		Si	
	NDIIMFP	NDSEP	NDIIMFP	NDSEP
ε_{pl}, eV	15.3	9.9	16.8	10.8
b, eV	4.7	5.8	10.3	9.5
$J_{ion\ 1}$, eV	75.9		100.5	
$J_{ion\ 2}$, eV	121.9		150.5	

$$x_{in}(\Delta) = \sum_{i=1}^{N_{pl}} \left[\lambda_{pl\ i} \cdot \frac{A_{pl\ i}\Delta^{\beta}}{\left(\Delta^2 - \varepsilon_{pl\ i}^2\right)^2 + b_i^{4-\alpha}\Delta^{\alpha}} \right] + \sum_{j=1}^{N_{ion}} \left[\lambda_{ion\ j} \cdot \frac{A_{ion\ j}}{\Delta^{2+a}} \eta\left(\Delta - J_{ion\ j}\right) \right], \quad (14)$$

with

$$\sum_{i=1}^{N_{pl}} \lambda_{pl\ i} + \sum_{j=1}^{N_{ion}} \lambda_{ion\ j} = 1$$

Here, η is the Heaviside step function, ε_{pl} is the energy of the plasmon, J_{ion} is the ionization energy, b is the plasmon damping parameter, λ_{pl} and λ_{ion} are the probabilities of the plasmon excitation and the ionization, respectively, while α and β are the fitting parameters. Their values for Al and Si are shown in Table I.

The coefficients Q_k are calculated for the bulk sample ($\tau_B \to \infty$) and for the surface layer of thickness τ_S. In Fig. 3, PES spectra for Si and Al calculated using Eqs. (1) and (7) are compared with the experimental data given in the XPS handbook[34]. The consistency between PES spectra and measurements allows us to apply the same strategy for shown PES calculation in the case of layers of finite thickness.

III. PES SPECTRA FOR FINITE THICKNESS LAYER

The angular distributions $Q_0(\tau, \mu_0, \mu, \varphi)$ are calculated using the SLA (9), the SAA (11), the numerical solution of Eqs. (1), (7) and Monte-Carlo simulations. The results corresponding to the single-layer model are shown in Fig. 4. From this figure it is apparent that the error of the SLA is decreasing when the layer thickness τ is increasing.

The following phenomenon is illustrated in Fig. 5. The X-ray beam strikes the surface normally, and the sighting angles of photo-electrons are 54.7° (so called "the magic angle") and 25°, respectively. For the "magic angle" scattering geometry, both SLA and SAA lead to satisfactory results with an error less than 10% for elastic peaks for 1 nm layer, and an error of about 3% for the semi-infinite layer for the whole energy range. However, for the 25°-scattering angle geometry, the SLA leads to significant

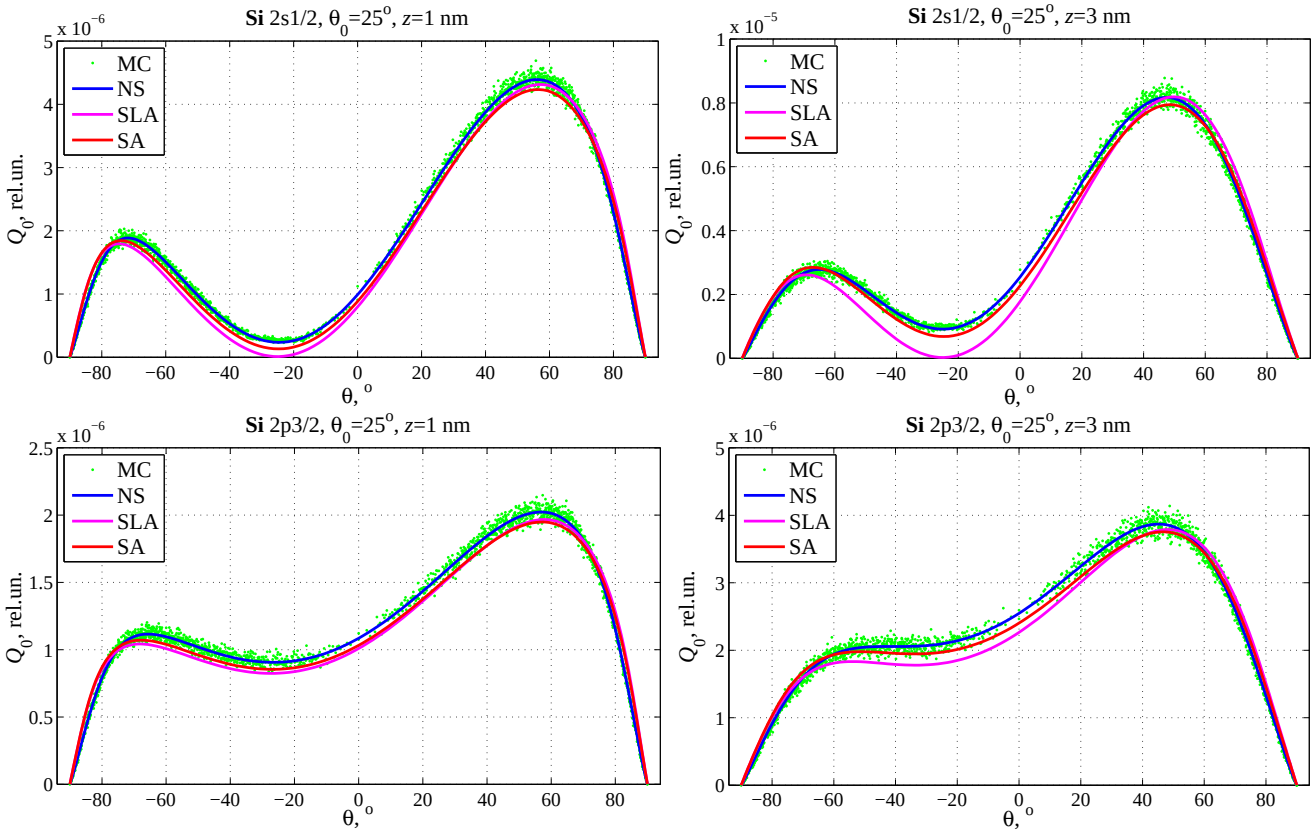

FIG. 4. (Color online) The angular distribution of the XPS peak intensity (Q_0) for layers of different thickness. (a) Si $2s_{1/2}$, $\theta_0 = 25^o$ and $z = 1$ nm, (b) Si $2s_{1/2}$, $\theta_0 = 25^o$ and $z = 3$ nm, (c) Si $2p_{3/2}$, $\theta_0 = 25^o$ and $z = 1$ nm, and (d) Si $2p_{3/2}$, $\theta_0 = 25^o$ and $z = 3$ nm. MC stands for Monte Carlo simulations ($4 \cdot 10^8$ particles are used), while NS stands for "numerical solution".

errors. The error for the silicone case can be up to 15% in the elastic peaks for a layer thickness of 1 nm, and of about 30% in the whole energy range for the semi-infinite layer. This fact should be taken into account in angular resolved XPS experiments. PES spectra computed by using the SLA and the SAA are closer when the layer thickness decreases. There are regions in the energy spectra where results of the SLA and the SAA differ from the exact numerical solution even for $\tau < 1$.

IV. CONCLUSIONS

It has been shown that the SAA [12,13,35] can be used together with MC-simulations and the SLA to analyze PES spectra. In contrast to the transport approximation[1,2], SAA is well-suited for layers of finite thickness.

The approach based on the numerical solution of Eqs. (7) and (13) is the most accurate and efficient. Equations (7) and (13) have been derived by using the invariant imbedding method.

The invariant imbedding method offers the possibility to derive appropriate equations for the coefficients Q_k, R_k and T_k avoiding the computations of the path length distribution function (PLDF).

In[20–23] there is a controversy regarding the photoelectron energy losses due to so-called intrinsic plasmon excitations. Essentially, it is stated that the intrinsic plasmon excitations are related to some electron photoionization effects. In this paper, computations of PES spectra for Al and Si (Fig. 3) have been performed without intrinsic plasmon excitations.

[1] C.J. Powell, A. Jablonsky, J. Electron. Spectrosc. **178-179**, 331 (2010).
[2] S. Tougaard, J. Electron. Spectrosc. **178-179**, 128 (2010).
[3] NIST, X-ray Photoelectron Spectroscopy Database, Version 4.1, http://srdata.nist.gov/xps.
[4] D. Chasoglou, E. Hryha, M. Norell, L. Nyborg, Appl. Surf. Sci. **268**, 496 (2013).
[5] L.P. Kazansky, L.A. Selyaninov, Yu.I. Kuznetsov, Appl. Surf. Sci. **259**, 385 (2012).
[6] S. Hajati, S. Tougaard, Journal of Surface Analysis. **15**, 220 (2009).
[7] S. Tougaard, J. Electron. Spectrosc. **52**, 243 (1990).
[8] I.S. Tilinin, W.S.M. Werner, Phys. Rev. B. **46**, 13739 (1992).
[9] V.P. Afanas'ev, D.S. Efremenko, D.A. Ivanov, P.S. Kaplya and A.V. Lubenchenko, Journal of Surface Investigation. X-ray, Synchrotron and Neutron Techniques. **7**, No.2, 382 (2012).
[10] A. Doicu and T. Trautmann, J. Quant. Spectrosc. Ra. **110**, 146 (2009).
[11] K. Stamnes, S. Tsay, W. Wiscombe and K. Jayaweera, Appl. Optics. **12**, 2502 (1988).
[12] S. Goudsmit, J.L. Saunderson, Physical Review. **57**, 24 (1940).

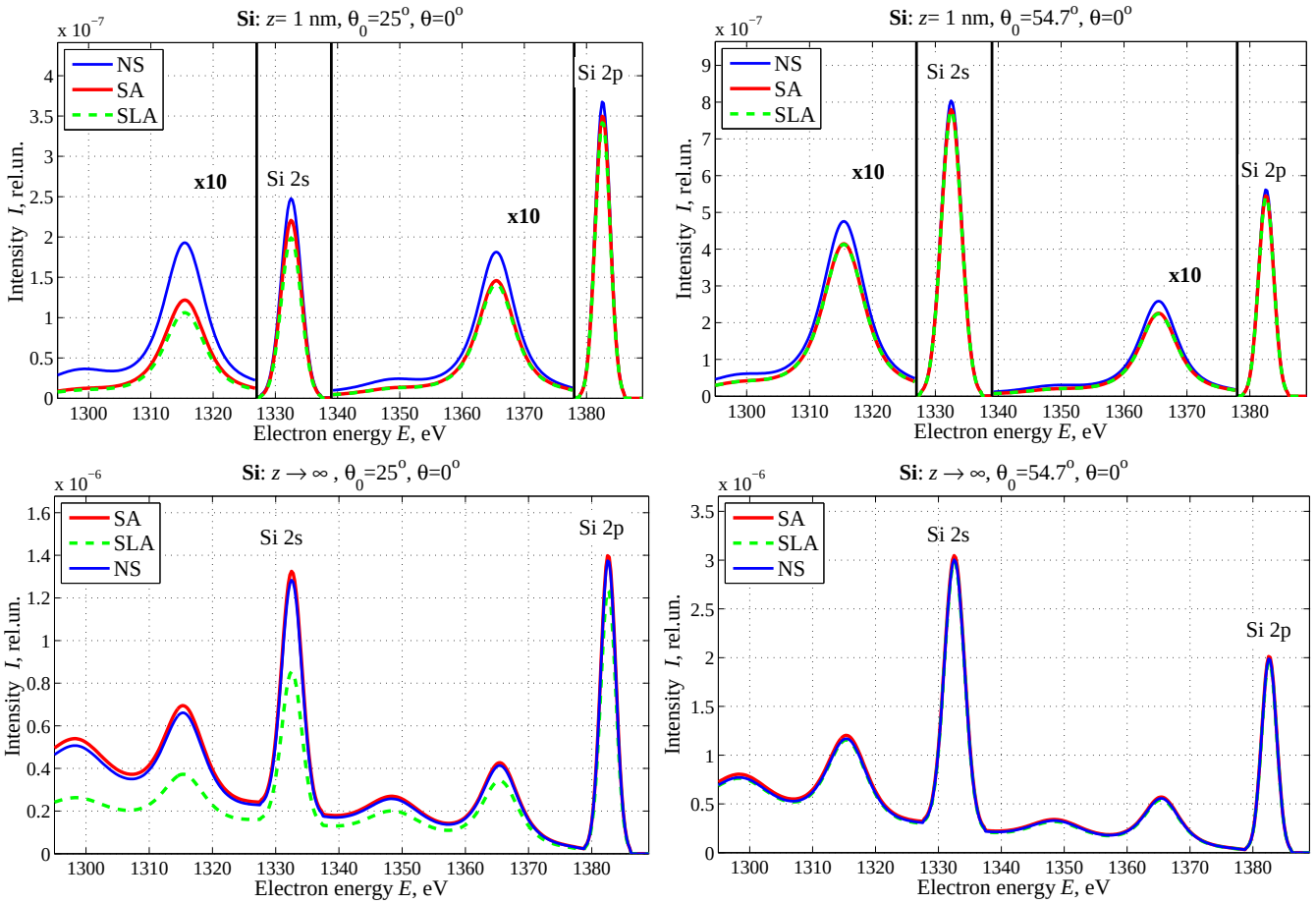

FIG. 5. (Color online) PES spectra Si for layer of different thickness and geometry. (a) $z = 1$ nm, $\theta_0 = 25^o$ and $\theta = 0^o$, (b) $z = 1$ nm, $\theta_0 = 54.7^o$ and $\theta = 0^o$, (c) $z \to \infty$, $\theta_0 = 25^o$ and $\theta = 0^o$, and (d) $z \to \infty$, $\theta_0 = 54.7^o$ and $\theta = 0^o$.

[13]S. Goudsmit, J.L. Saunderson, Physical Review. **58**, 36 (1940).
[14]V.V. Sobolev, Light Scattering In Planetary Atmospheres. [1st ed.] Oxford: Pergamon Press, 1975.
[15]L. Landau, J.Phys. **8**, 201 (1944).
[16]S. Tougaard and I. Chorkendorff. Phys. Rev. B. **35**, 6570 (1987).
[17]S. Tougaard, J. Kraaer, Phys. Rev. B. **43**, 1651 (1991).
[18]V.P. Afanas'ev, A.V. Lubenchenko, Surface Investigation. **13**, 1087 (1998).
[19]A.N. Tikhonov, V.Ja. Arsenin, Method of the solution of incorrect problems. Nauka, Moscow [in Russian].
[20]B.I. Lundqvist, Phys. Kondens. Mater. **9**, 236 (1969).
[21]D.C. Langreth, Phys. Rev. Lett. **26**, 1229 (1971).
[22]F. Ybero, S. Tougaard, Phys. Rev. B. **71**, 045414 (2005).
[23]C. Biswas, A.K. Shukla, S. Banik, V.K. Ahire, S.R. Barman, Phys. Rev. B. **67**, 165416 (2003).
[24]V.P. Afanas'ev, D.S. Efremenko and A.V. Lubenchenko, Light Scattering Reviews 8. **XXV**, 632 (2013).
[25]V.P. Afanas'ev, D.S. Efremenko, A.V. Lubenchenko et al. Bulletin of the Russian Academy of Sciences: Physics. **74**, No.2, 170 (2010).
[26]V. Afanas'ev, A. Lubenchenko, M. Gubkin, Eur. Phys. J. B. **37**, 117 (2004).
[27]M. Trzhaskovskaya, V. Nefedov, Y. Yarzhemsky, Atom. Data Nucl. Data. **77 (1)**, 97 (2001).
[28]M. Trzhaskovskaya, V. Nefedov, Y. Yarzhemsky, Atom. Data Nucl. Data. **82 (2)**, 257 (2002).
[29]J. Peinado, J.J. Ibez, V. Hernadez, E. Arias, Procedia Computer Science. **1**, 2569 (2010).
[30]A. Jablonski, F. Salvat, C.J. Powell. NIST Electron Elastic Scattering Cross Section Database, Version 3.2, Standard Reference Data Program Database 64 and http://www.nist.gov/srd/nist64.cfm.
[31]S. Tanuma, C.J. Powell, D.R. Penn, Surf. Interface Anal. **17**, 911 (1991).
[32]S. Tanuma, C.J. Powell, D.R. Penn, Surf. Interface Anal. **35**,268 (2003).
[33]V.P. Afanas'ev, P.S. Kaplya, A.V. Lubenchenko, O.I. Lubenchenko, Vacuum. **105**, 96 (2014).
[34]C. Wagner, W. Riggs, L. Davis, J. Moulder, Handbook of X-ray Photoelectron Spectroscopy, Perkin-Elmer Corporation, Physical Electronics Division, USA, 1979.
[35]W. Scott, Rev. Mod. Phys. **35**, 231 (1963).